



HAL
open science

Gamma-response characterization of a solution-grown stilbene based detector assembly in the 59 keV–4.44 MeV energy range; an alternative low-resolution gamma spectrometer

Augusto Di Chicco, Alix Sardet, Michaël Petit, Robert Jacqmin, Vincent Gressier, Brian Stout

► To cite this version:

Augusto Di Chicco, Alix Sardet, Michaël Petit, Robert Jacqmin, Vincent Gressier, et al.. Gamma-response characterization of a solution-grown stilbene based detector assembly in the 59 keV–4.44 MeV energy range; an alternative low-resolution gamma spectrometer. Nuclear Instruments and Methods in Physics Research Section A: Accelerators, Spectrometers, Detectors and Associated Equipment, 2022, 1034, pp.166740. 10.1016/j.nima.2022.166740 . irsn-04666496

HAL Id: irsn-04666496

<https://irsn.hal.science/irsn-04666496v1>

Submitted on 13 Nov 2024

HAL is a multi-disciplinary open access archive for the deposit and dissemination of scientific research documents, whether they are published or not. The documents may come from teaching and research institutions in France or abroad, or from public or private research centers.

L'archive ouverte pluridisciplinaire **HAL**, est destinée au dépôt et à la diffusion de documents scientifiques de niveau recherche, publiés ou non, émanant des établissements d'enseignement et de recherche français ou étrangers, des laboratoires publics ou privés.



Distributed under a Creative Commons Attribution - NonCommercial 4.0 International License

1 Title

2 Gamma-response characterization of a solution-grown stilbene based detector assembly in the 59 keV
3 - 4.44 MeV energy range; an alternative low-resolution gamma spectrometer

5 Authors

6 Augusto Di Chicco^{a,d}

7 Alix Sardet^{b*}

8 Michaël Petit^c

9 Robert Jacqmin^a

10 Vincent Gressier^c

11 Brian Stout^d

12
13 ^aCEA, DES, IRESNE, DER, 13108 Saint-Paul-Lez-Durance CEDEX France

14 ^bCEA, DES, IRESNE, DTN, SMTA, LMN, 13108 Saint-Paul-Lez-Durance CEDEX France

15 ^cIRSN Cadarache, SDOS/LMDN, 13115 Saint-Paul-Lez-Durance, France

16 ^dAix-Marseille University, Institut Fresnel - UMR 7249, 13397 Marseille, France

17

18 ***Corresponding Author.** Tel: +33 4 42 25 26 57. E-mail address: Alix.SARDET@cea.fr

19

20 Abstract

21 The photon response characterization of a Ø 25.4 mm × 25.4 mm solution-grown stilbene based
22 detector assembly was performed in the 59 keV - 4.44 MeV energy range. Energy calibration was
23 carried out using not only direct measurements but also via coincidence measurements in order to
24 obtain more reliable results. Both methods gave consistent results. To establish an accurate model of
25 the detector, its energy resolution was determined and included in MCNPX-PoliMi simulations. This
26 model served to compute the gamma-response matrix in the 0.1-7.3 MeV energy range. This matrix
27 was used as an input of the GRAVEL spectrum unfolding code when attempting to unfold the
28 measured spectra of well-known sources. Despite a few discrepancies concerning peak intensities, the
29 main gamma peaks were successfully identified in the 0.059-4.4 MeV energy range, thus confirming
30 the utility of solution-grown stilbene as a low-resolution gamma spectrometer, especially for
31 identifying the gamma component in neutron fields.

32 Keywords

33 Organic scintillator detector, solution-grown stilbene, energy calibration, γ -ray response matrix,
34 spectra unfolding, GRAVEL, crystal scintillator, gamma spectrometer.

35

36

37 1 INTRODUCTION

38 Detectors based on organic scintillators are widely used in the field of fast neutron spectroscopy. Their
39 popularity stems from their high detection efficiencies, sufficient energy resolution, and, for most
40 types, their ability to discriminate neutrons and gamma rays via pulse shape discrimination (PSD)
41 above a minimum threshold. While liquid scintillators, such as BC501A/NE213 [1][2][3], are the most
42 commonly used due to their low production costs and the ease in which they are produced in large
43 volumes, recent developments in solution-growth techniques have made it possible to produce high-
44 quality single organic crystals of various hydrocarbonated compounds at a modest price. These
45 developments revived an interest in crystal scintillators, such as stilbene, to use as neutron
46 spectrometers covering an energy range from ~100 keV [4] to ~20 MeV in order to monitor spectra
47 produced in beam facilities or zero-power experimental nuclear reactors.

48 The work presented in this paper is part of a larger study dedicated to assessing the neutron
49 spectrometry performance of a \varnothing 25.4 mm \times H 25.4 mm stilbene ($C_{14}H_{12}$) detector assembly. A part of
50 the gamma response, typically between \sim 340 keV and \sim 1.550 MeV, must be characterized so that it
51 can be used to calibrate the neutron response. Nevertheless, carrying out a gamma characterization
52 over a wider energy range can also be useful for determining the gamma component accompanying
53 any neutron field.

54 To this end, two energy calibration techniques, one with direct measurements and one with
55 coincidence measurements, were used to determine the calibration curve. A MCNPX-PoliMi model of
56 the detector was built to help accurately determine the energy resolution of the detector. This model
57 also served to construct the gamma response matrix of the detector, which was then used as an input
58 parameter of the GRAVEL unfolding code for carrying out the deconvolution of experimental spectra
59 of well-known gamma sources.
60

61 **2 EXPERIMENTAL DETAILS**

62 **2.1 ORGANIC SCINTILLATOR DETECTORS**

63 Two cylindrical organic scintillators, listed in Table 1, are used in this work. The main detector is a
64 \varnothing 25.4 mm \times 25.4 mm solution-grown [5] stilbene, produced by InradOptics [6] and encapsulated in a
65 0.5 mm thick aluminum cylinder. The other detector is only used to perform coincidence
66 measurements and will not be described further. In earlier works [4] [7], the high voltage of the main
67 detector was set to measure low energy neutrons (e.g. -1230 V to measure neutrons below 1 MeV). In
68 the present work, as the goal was to accommodate a neutron energy range as wide as possible (up to
69 17 MeV), the high voltage was set to -930 V, which corresponds to a gain reduction factor of about 40.
70

71 INSERT TABLE 1 HERE
72

73 **2.2 DATA ACQUISITION AND ANALYSIS**

74 Data acquisition was performed using a CAEN DT5730 digital acquisition (DAQ) system [10], with
75 8.MCX data acquisition channels, 14-bit resolution, a 2-V maximum digitization window and a
76 500.MHz sampling rate. Digital acquisition systems offer many advantages compared to analog
77 systems, such as an ease of assembly, the capacity to timestamp at picosecond each triggering signal
78 with a measured 1.ns resolution from DT5730's capability [4], an ability to support high count rates
79 and enhanced neutron/gamma discrimination capabilities [11] [12]. After digitization, anode signals
80 from the photomultipliers are processed by the Digital Pulse Processing - Pulse Shape Discrimination
81 (DPP-PSD) firmware. This firmware timestamps the signals and computes two integrals over two
82 different time-windows: one integral is called Long gate (Q_L) and covers most of the signal, while the
83 other is called Short gate (Q_S) and covers only the fast part of the signal. The ratio of these two
84 integrals provides our PSD information.

85 The data recorded are: time of radiation detection, Q_L , Q_S , flags (firmware information about the signal
86 recording status) and, if the "wave" mode is selected, the digitized signal itself. This last capacity was
87 not used routinely as it requires considerable computational power, reduces the maximum count rate
88 that the system can handle, and drastically increases data management and analysis requirements. All
89 data produced in this work are processed and analyzed using the ROOT framework [13].
90

91 **2.3 EXPERIMENTAL SETUPS**

92 In order to perform a complete gamma characterization of the stilbene detector, two sets of
93 experiments were performed using several sources (see Table 2) available at the AMANDE facility
94 [14]. The $^{12}C^*$ first excited state decay of the $^{241}AmBe$ neutron-gamma source [15] produces 4.438
95 MeV gamma rays, which primarily interact with the matter through Compton scattering and pair
96 production, thus producing a usable double escape peak at 3.416 MeV and a Compton edge.

97
98
99

INSERT TABLE 2 HERE

100 2.3.1 Direct measurements

101 For direct measurement, each gamma source was positioned at 100 mm from the detector front face to
102 ensure a high number of counts in a reasonable amount of time with a relatively homogeneous detector
103 irradiation, while avoiding too many pile-up events.

104

105 2.3.2 Coincidence measurements

106 A known, but seldom-used energy calibration method is based on a gamma scattering coincidence
107 technique [17] [18] [19] [20]. As shown in Figure 1, , for such measurements, the front face of the
108 $\text{Ø } 25.4 \times 25.4 \text{ mm}^3$ stilbene detector was placed at 240 mm from the front face of a $\text{Ø } 50.8 \times 50.8 \text{ mm}^3$
109 stilbene detector, with their cylindrical axis being aligned. Gamma sources were placed inside a
110 hollow lead cylinder (inner radius of 70 mm), at a distance of around 60 mm below the stilbene
111 crystal, which was thus uniformly irradiated. Since the sources used can emit several gamma
112 simultaneously, lead shielding was used to avoid direct and undesirable coincidences on the second
113 detector. The coincidence window between the two detectors was set to 60 ns. According to the solid
114 angle of the experimental set-up, only gamma rays that interacted with the main stilbene detector with
115 a scattering angle around 90° (within $\pm 9^\circ$) could induce the expected coincidences. The associated
116 uncertainty on the deposited energy varies with the incident gamma ray's energy and reaches a
117 maximum of $\sim 9\%$ around 500 keV ($\sim 7\%$ at 1500 keV).

118

119

INSERT FIGURE 1 HERE

120

121 3 ENERGY CALIBRATION

122 Energy calibration of a scintillator is performed by associating the known energy of a photoelectric
123 peak, of a Compton Edge (CE) or of simple/double-escape peak to the corresponding discrete channel
124 of the measured spectrum. However, due to the finite energy resolution of the detector, the exact
125 position of the CE is not always easily identifiable. Figure 2 presents the ^{207}Bi (a) and ^{60}Co (b) spectra
126 obtained with the $\text{Ø } 25.4 \times 25.4 \text{ mm}^3$ stilbene detector with (red solid line) and without (blue solid
127 line) the coincidence method. Given the experimental setup described in section 2.3, in coincidence
128 mode, each peak is induced by a gamma ray of given energy.

129

130

INSERT FIGURE 2 HERE

131

132 3.1 DIRECT MEASUREMENTS

133 In this work, an approach similar to that used to identify the distribution of recoil protons was used
134 [21] to determine the CE position for direct measurements. Indeed, given the shape of the ideal
135 spectrum (sharp drop at the CE position), and irrespective of energy resolution effects, the first-order
136 derivative is assumed to take the form of an inverse Gaussian distribution, centered on the position of
137 the CE (see Figure 3). Such a method was also used in previous works by [22] [23] [24].

138

139

INSERT FIGURE 3 HERE

140

141 In the energy range between 0.3 MeV and 2 MeV, the relationship between the integral charge (i.e.
142 channel) and the energy deposited by gamma rays is almost linear (see black dashed line on Figure
143 4(a.1)) [25]. Therefore, the calibration curve, denoted L_{Mean} , can be described using a first-order
144 polynomial:

145 $L(\text{MeVee}) = b \cdot PH(\text{channel}) + a$ (1)

146 where a and b are parameters determined by fitting the calibration data points. Obtained values are
 147 respectively $b = (38.59 \pm 0.26) \times 10^{-4}$ and $a = (2.1 \pm 0.4) \times 10^{-2}$ for a χ^2/ndf^1 of $1.063 \times 10^{-4}/6$.

148 However, for energies below 0.3 MeV and above 2 MeV, a simple linear fit is no longer sufficient to
 149 reproduce the stilbene's gamma ray response and a second-order polynomial is considered:

150 $L(\text{MeVee}) = c \cdot PH^2(\text{channel}) + b \cdot PH(\text{channel}) + a$ (2)

151 where a , b and c are parameters determined by fitting the calibration data points.

152 At low energy, calibration was performed using data from ^{241}Am as the starting point. This data was
 153 completed by a point at 0.344 MeV ($E_{re}(180^\circ) = 0.197$ MeV), obtained using a ^{152}Eu source. The
 154 low-energy calibration curve is denoted L_{Low} (solid red line on Figure 4(a.2)) and its parameters, using
 155 the notation from Eq. (2), are $a = 0$ (imposed value), $b = (41.5 \pm 0.5) \times 10^{-4}$ and $c = (-7.77 \pm 2.16) \times 10^{-7}$.
 156 The associated χ^2/ndf value ($1.714 \times 10^{-5}/2$) indicates a better data/model agreement than for the
 157 previous L_{Mean} result ($\chi^2/\text{ndf} = 4.203 \times 10^{-5}/2$ in the same energy range). Similarly, to improve the
 158 calibration process at high energy, the double escape peak at 3.416 MeV induced by the 4.438 MeV
 159 gamma of $^{12}\text{C}^*$ was included in the data set. The associated calibration curve is denoted L_{High} (see
 160 blue solid line on Figure 4(a.1)) and its parameters are $a = (3.4 \pm 0.6) \times 10^{-2}$, $b = (38 \pm 0.3) \times 10^{-4}$ and
 161 $c = (-9.1 \pm 2.8) \times 10^{-8}$. The obtained χ^2/ndf is $2.105 \times 10^{-5}/2$, which indicates, even for high energies, a
 162 slightly better data/model agreement than for L_{Mean} result ($\chi^2/\text{ndf} = 3.849 \times 10^{-5}/3$ in the same energy
 163 range).

164 As can be seen on Figure 4(b), when comparing spectra calibrated using L_{Mean} and L_{High}
 165 (resp. L_{Low}), discrepancies are obtained on the CE (resp. photoelectric peak) position. Using L_{Mean} ,
 166 the 59.6 keV peak of ^{241}Am is overestimated by 33.2% and the 4.196 MeV CE of $^{12}\text{C}^*$ by 2%.
 167 Therefore, using a purely linear calibration curve (i.e. L_{Mean}) would result in a significant bias in the
 168 low (< 0.3 MeV) and a small but real bias in the high (> 2 MeV) energy ranges. The observed non-
 169 linearity may have several origins, among which the PMT, the non-linearity of the electron light and
 170 the derivative-Gaussian fit method used to determine the CE position. Regarding the latter,
 171 comparison to coincidence measurements (see Section 3.2) suggests that it is not the main source of
 172 non-linearity.

173
 174 INSERT FIGURE 4 HERE
 175

176 3.2 COINCIDENCE MEASUREMENTS

177 As shown in Figure 2, in coincidence measurements, the recorded spectra take the shape of Gaussian
 178 distribution, centered on the energy deposited by gamma rays scattering at 90° . Since the energy of
 179 these photons is lower than that of photons scattered at 180° (see Table 2, $E_{re}(90^\circ)$) the calibration
 180 point is obtained for lower energies, and thus lower channels, than with a direct measurement.

181 The main advantage of the coincidence configuration is that, for each source, the peak positions
 182 correspond to well-known energies, thus giving a direct calibration curve. As this calibration does not
 183 depend on any assumption (for instance the position of the CE), it can be used to assess the accuracy
 184 of other calibration methods, such as the derivative method used in the previous section. However, its
 185 main drawback is that it requires about 200 times longer measurement times than direct measurements
 186 in order to acquire sufficient data for a reliable measurement. Given the available sources (see Table
 187 2), this calibration could only be established for energies below 2 MeV. For energies below 0.3 MeV,
 188 the obtained calibration points exhibit the same non-linear behavior as that observed during direct

¹ Ndf (number of degrees of freedom) = number of data points – number of fitting function parameters (for the ROOT framework)

189 measurements. This proves the cause of the non-linear behavior is not to be found in the used
190 derivative method. A parametrization with a second-order polynomial function below 0.3 MeV and a
191 first-order polynomial up to 2 MeV was used to account for this non-linearity.
192

193 3.3 PERFORMANCE COMPARISON OF CALIBRATION METHODS

194 Calibration curves obtained for direct (black solid square) and coincidence (black empty square)
195 measurements are presented on Figure 5 (left). Corresponding equation parameters are presented in
196 Table 3. Overall, the obtained curves present an excellent agreement with parameters compatible
197 within uncertainties and a maximum deviation of 1.54% at 0.138 MeV. Figure 5 (right) compares the
198 experimental spectrum of ^{60}Co calibrated with (blue solid line) and without (red solid line) the
199 coincidence method. Compared to the reference energies of ^{60}Co , there are shifts of 0.38% and 0.57%
200 at 1.173 MeV and of 0.08% and 0.35% at 1.332 MeV with and without the coincidence method,
201 respectively.
202

203 INSERT FIGURE 5 HERE

204
205
206 INSERT TABLE 3 HERE
207

208 Results obtained by the direct and coincidence methods are in good agreement and both techniques
209 provide an accurate calibration curve. Since direct measurements are much easier and faster, this
210 approach will be kept for future work.
211

212 4 MCNPX SIMULATIONS

213 To simulate stilbene's gamma ray response, the MCNPX Monte Carlo code has been chosen. It is used
214 in photon-electron mode with the ENDF/B-VI photo-atomic data libraries to define material
215 properties. The constructed geometric model is a simple one, which includes the stilbene crystal, its
216 aluminum container, the Plexiglas light-guide and the PMT container, which was filled only with air.
217 As mentioned in the previous section, organic scintillators have a finite energy resolution, which one
218 must account for in order to perform accurate simulations. To this end, a Gaussian Energy Broadening
219 (GEB) [27] function can be applied to simulation results.
220

221 4.1 ENERGY RESOLUTION

222 The GEB function is expressed as a function of $FWHM$, which is written as:

$$223 FWHM(E) = L(E) \cdot R(L(E)) = a' + b' \sqrt{E + c'E^2} \quad (3)$$

224 In Eq.(3), $L(E)$ represents the light-output and $R(L(E))$ the associated energy resolution, a' , b' and c'
225 are parameters. From the empirical formula (1) [28]:

$$226 R(L(E)) = \frac{\Delta L(E)}{L(E)} = 1.5 \cdot \frac{L_{1/2} - L_{MAX}}{L_{1/2}} \quad (4)$$

227 where L_{MAX} corresponds to the energy of the maximum counts (around the Compton edge) and $L_{1/2}$
228 to the energy where this count is halved, a first estimation of $R(L(E))$ for the different sources listed
229 in Table 2 was performed. Using the Pulse Height (F8) tally of MCNPX, ideal Compton spectra were
230 computed and then convolved using the GEB function parametrized with the results from equation (3).
231 Discrepancies were observed between simulations and experimental spectra, with an overestimation of
232 $R(L(E))$. Therefore, the $R(L(E))$ value was fixed and manually adjusted until a good agreement was

233 reached between experimental and simulated data at the CE level. Afterwards, to expand $R(L(E))$
234 over the whole range of interest, data points thus obtained were fitted using the standard function [28]:

$$235 \quad R(L(E)) = \sqrt{\alpha^2 + \frac{\beta^2}{L(E)} + \left(\frac{\gamma}{L(E)}\right)^2} \quad (5)$$

236 in which the α , β and γ parameters respectively account for the light transmission from the scintillator
237 to the photocathode, the statistical variation of the photoelectron production mechanism, and the noise
238 contributions of the acquisition system. Eq. (3) and (5) parameters, which are listed in Table 4, were
239 obtained by fitting the experimental data as shown in Figure 6. For the determination of the energy
240 resolution at 4438 keV and referring to [29], we have accounted for an “apparent” resolution of 90
241 keV (± 4 .keV) arising from the Doppler broadening effect.

242
243 INSERT FIGURE 6 HERE

244
245 INSERT TABLE 4 HERE

246 247 4.2 DIRECT MEASUREMENTS SIMULATIONS

248 Figure 7 presents the comparison between calibrated experimental spectra (blue solid line), after
249 background subtraction, and simulated (black dashed line), accounting for the stilbene’s energy
250 resolution, spectra of the ^{22}Na (a) and ^{207}Bi (b) sources. Experimental spectra are in good agreement
251 with simulated results (less than 1% deviation on the position of the CE). Nevertheless, the simulation
252 does not reproduce the experimentally observed Compton continuum. Non-modelled materials, such
253 as the experiment table or the PMT’s components, which create backscatter contributions, could
254 explain such a discrepancy.

255
256 INSERT FIGURE 7 HERE

257 258 4.3 COINCIDENCE MEASUREMENT SIMULATIONS

259 Since the F8 tally does not enable the selection of gamma rays scattered at a specific angle (90° in this
260 work), a modified version of the code, MCNPX-PoliMi (Polytechnic of Milano) [30], was used
261 instead. Similarly, to the PTRAC option of MCNPX, MCNPX-PoliMi generates an output file that
262 records, for each simulated history, information about collision events within a user-chosen cell.
263 Among the recorded information, the particle type, deposited energy, number of collisions and
264 incident energy of the interacting particle are of interest to our study. These data were processed using
265 the MPPost (MCNPX-Polimi Post-Processor) software, developed by the same team [31], in order to
266 account for the detector response.

267 Figure 8 shows the comparison between calibrated experimental and simulated broadened spectra of
268 ^{60}Co (a) and ^{152}Eu (b) sources. For both sources, the positions of the energy peaks in the experimental
269 spectra are in good agreement with that of the simulated spectra. However, discrepancies can be
270 observed on either side of the peak tails. A probable cause is that random coincidences and recoil
271 electrons, which are not correctly simulated [32], are not accounted for.

272
273 INSERT FIGURE 8 HERE

274
275 Despite a few discrepancies, simulated spectra present a good agreement with experimental ones.
276 Table 5 lists the obtained deviations on both the energy and the FWHM for each measured gamma ray.
277 While the recoil electron energy is relatively well reproduced, with a maximum deviation of about 1%
278 at 79.keV, the FHWM presents more significant deviations (up to 7% on the 0.63 MeV gamma ray
279 from the ^{152}Eu source). The most probable origin of these discrepancies is the simplified model of the

280 experiment, which does not reproduce the background caused by photon scattering, nor an eventual
281 small shift in the source position.

282
283
284

INSERT TABLE 5 HERE

285 **5 GAMMA RESPONSE MATRIX AND SPECTRUM UNFOLDING**

286 **5.1 RESPONSE MATRIX CONSTRUCTION AND INTRINSIC EFFICIENCY**

287 For organic scintillators, as for many other detectors, the relationship between the incident particle
288 flux $\phi(E)$ and the measured response $PH(L)$ can be formally expressed as:

$$289 \quad PH(L) = \int_0^{\infty} R(E, L)\phi(E)dE \quad (6)$$

290 where $R(E, L)$ is the response matrix, *i.e.* the mathematical operator that contains the relevant
291 normalized responses of the organic scintillator in its operational energy range, and thereby accounts
292 for its energy resolution. The gamma-ray response matrix of the stilbene detector was constructed by
293 performing 240 pointwise isotropic gamma simulations, each with 10^9 particles emitted by a source
294 placed at 100 mm from the detector front face. The response matrix was constructed between 100 keV
295 and 7.3 MeV (*i.e.* 30 keV/bin), each calculation yielding a simulated response between 0 and 8
296 MeVee, tallied over 1024 bins. It is necessary to point out the calculated response matrix is an ideal
297 one and in practice, the gamma scattering around the detector should be subtracted in order to
298 correctly deduce an incident spectra $\phi(E)$.

299 The intrinsic gamma-ray efficiency $\varepsilon(E)$ curve can be computed from the response matrix according to
300 equation (7):

$$301 \quad \varepsilon(E_i) = \int_{L_{th}}^{L_M} R(E_i, L)dL \quad (7)$$

302 where $R(E_i, L)$ is the gamma ray response at the incident energy (E_i). L_M and L_{th} (in MeVee) are
303 respectively the maximum and the threshold light output. Figure 9 shows, for four different threshold
304 values, the calculated gamma efficiency curve of the stilbene up to 3 MeV. Results are in rather good
305 agreement with experimental values obtained with a ^{137}Cs (0.662 MeV) source. Above a 0.1 MeVee
306 threshold, discrepancies observed remain below 1.6%. These discrepancies could be slightly reduced
307 by improving the MCNPX model used to construct the gamma response matrix (*i.e.* by a better
308 reproduction of the Compton continuum).

309
310
311

INSERT FIGURE 9 HERE

312

313 **5.2 SPECTRA UNFOLDING WITH GRAVEL ALGORITHM**

314 Unfolding (or deconvolution) is a procedure that addresses the inverse problem in Eq. (6), *i.e.* that
315 gives the energy flux $\phi(E)$ which generated the scintillator response $PH(L)$. Over the years, many
316 methods and codes have been developed for this operation [33] [34]. In this work, the iterative code
317 GRAVEL was chosen as it is widely used for unfolding spectra for both gamma rays [1] [35] and
318 neutrons [36] [37]. GRAVEL uses an iterative algorithm based on the nonlinear least-squares method
319 and only yields physically meaningful solutions (*i.e.* an everywhere positive flux). To start the
320 iterative process, GRAVEL needs the experimental spectrum to be unfolded, the response matrix, an
321 input flux (as a first solution to start the iterations), the maximum number of iterations to be performed
322 and a χ^2 target. The code runs until either the maximum number of iterations or the defined χ^2 target
323 value is reached. For all tested spectra, 50000 iterations were performed using a flat (all bins equal to
324 1) input flux. Tests were performed to ensure that using such an input flux did not yield significant
325 changes in the result compared to what is obtained when using a realistic input flux. The choice of

326 50000 iterations depends on the fact that for all tested sources they guarantee the minimum and stable
327 χ^2 value.

328 Gamma spectra unfolded by GRAVEL are compared with known theoretical peaks [16], in terms of
329 peak average energy and emission intensity in order to assess the quality of the performed unfolding.
330 Figure 10 presents the comparison results for $^{12}\text{C}^*$ (a) and ^{152}Eu (b). Experimental spectra were scaled
331 to match the peak of highest emission intensity. Observed deviations on the peak energies and their
332 emission intensities are reported in Table 6.

333

334

INSERT FIGURE 10 HERE

335

336

INSERT TABLE 6 HERE

337

338 For $^{12}\text{C}^*$, there is a deviation of 0.24% between the measured and theoretical energies. In addition,
339 sporadic peaks are present at lower energies, probably caused by gamma scattering around the
340 detector. For ^{152}Eu , given the large number of energetically-close gamma lines (over 40 lines of
341 similar intensities in the [0.45-0.7] MeV range for example) and the finite resolution of the stilbene
342 detector, only 13 lines above 1% intensity could be considered. Indeed GRAVEL algorithm can't, in
343 this case, unfold properly low intensity gamma rays which are too energetically-close. In this study,
344 the limit is around 1%. Moreover, in the intervals 0.411-0.444 MeV, 1.085-1.112 MeV and 1.212-
345 1.299 MeV, measurements are compared to the average of the theoretical peaks, weighted by their
346 respective intensities, as the resolution of the detector was not good enough to separate the
347 contributions. While deviations from the expected mean energies are less than 1%, deviations on peak
348 intensities can reach up to 87.92% on the peak of lowest energy (0.244 MeV). These deviations are
349 related to both the complexity of ^{152}Eu source and the uncertainties associated to the stilbene response
350 matrix. Nevertheless, unfolding a stilbene gamma spectrum permits, with sufficient accuracy, a peak
351 identification, even for a complex source, thus demonstrating its capacity as a gamma spectrometer.

352

353 6 CONCLUSIONS

354 In this work, the complete gamma characterization of a \emptyset 25.4 mm \times 25.4 mm solution-grown stilbene
355 based detector assembly has been performed. Gamma sources covering an energy range between
356 0.059 MeV and 4.438 MeV were used to determine the energy resolution of the detector and perform
357 its energy calibration. For the latter, consistent results were obtained between coincidence
358 measurements and direct measurements, thus showing that applying a first-derivative method to
359 determine the position of the Compton edge is accurate and reliable for calibration purposes.
360 Nevertheless, as non-linearities were observed below 0.3 MeV and above 2 MeV, the calibration curve
361 had to be adapted by introducing second-order polynomials in these ranges in order to use the stilbene
362 as a broadband gamma spectrometer. Simulations were performed using a simple MCNPX-PoliMi
363 model. They successfully reproduced the expected detector behavior around the Compton Edge,
364 although the experimental Compton continuum could not be reproduced, probably because of the
365 rather simple MCNP model used. The gamma-ray response matrix of the detector was built and the
366 intrinsic efficiency curve computed for several thresholds. To validate the constructed matrix, spectra
367 of known sources were unfolded using the GRAVEL iterative code. Results showed that the
368 constructed matrix is sufficient to successfully identify the main gamma peaks present in the spectrum
369 in the energy range between 0.059 and 4.4 MeV. These studies have demonstrated the capabilities of
370 stilbene based detectors to serve as a low-resolution gamma spectrometer in the energy range between
371 0.059 and 4.4 MeV. Future work will focus on the neutron response characterization of this detector
372 assembly, using monoenergetic neutrons produced by the AMANDE facility and a white neutron
373 spectrum produced by the PTB cyclotron [38]. The main objective of these measurements will be to
374 obtain measured [39] [40] and, if possible, the simulated [41] neutron response matrices of the
375 detector assembly to assess its performance as a broadband neutron spectrometer in mixed radiation

376 fields. In addition, as part of these measurements, anisotropy effects of the stilbene crystal [42] [43]
377 will be investigated in more details as well as their impact on the neutron response.

378

379 **Acknowledgments**

380 This project has received funding from the European Union's Horizon 2020 research and innovation
381 program under grant agreements N° 847594 (ARIEL) and 847552 (SANDA).

382

383 **References**

- 384 [1] H. Klein et S. Neumann, « Neutron and photon spectrometry with liquid scintillation detectors in
385 mixed fields », *Nucl. Instrum. Methods Phys. Res. Sect. Accel. Spectrometers Detect. Assoc.*
386 *Equip.*, vol. 476, n° 1, p. 132-142, janv. 2002, doi: 10.1016/S0168-9002(01)01410-3.
- 387 [2] R. Batchelor, W. B. Gilboy, J. B. Parker, et J. H. Towle, « The response of organic scintillators to
388 fast neutrons », *Nucl. Instrum. Methods*, vol. 13, p. 70-82, août 1961, doi: 10.1016/0029-
389 554X(61)90171-9.
- 390 [3] W. R. Burrus et V. V. Verbinski, « Fast-neutron spectroscopy with thick organic scintillators »,
391 *Nucl. Instrum. Methods*, vol. 67, n° 2, p. 181-196, janv. 1969, doi: 10.1016/0029-554X(69)90446-
392 7.
- 393 [4] A. D. Chicco, M. Petit, R. Jacqmin, V. Gressier, et B. Stout, « Investigation of the neutron-gamma
394 ray discrimination performance at low neutron energy of a solution-grown stilbene scintillator »,
395 *EPJ Web Conf.*, vol. 225, p. 04013, 2020, doi: 10.1051/epjconf/202022504013.
- 396 [5] N. P. Zaitseva *et al.*, « Neutron detection with single crystal organic scintillators », San Diego,
397 CA, août 2009, p. 744911. doi: 10.1117/12.829870.
- 398 [6] « Inrad Optics, Advanced Optical Materials, Design and Manufacturing ». <https://www.inradoptics.com/> (consulté le 23 avril 2020).
- 399 [7] L. Dioni, V. Gressier, G. Nardin, R. Jacqmin, B. Stout, et M. Sumini, « Tests of a solution-grown
400 stilbene scintillator in mono-energetic neutron beams of 565 keV and 5 MeV », *Nucl. Instrum.*
401 *Methods Phys. Res. Sect. Accel. Spectrometers Detect. Assoc. Equip.*, vol. 880, p. 210-215, févr.
402 2018, doi: 10.1016/j.nima.2017.06.048.
- 403 [8] « 9214B Series - ET-Enterprises Ltd ». [http://et-](http://et-enterprises.com/products/photomultipliers/product/p9214b-series)
404 [enterprises.com/products/photomultipliers/product/p9214b-series](http://et-enterprises.com/products/photomultipliers/product/p9214b-series) (consulté le 5 mai 2019).
- 405 [9] « 9266B Series - 51 mm Photomultiplier - ET-Enterprises Ltd ». [https://et-](https://et-enterprises.com/products/photomultipliers/product/p9266b-series)
406 [enterprises.com/products/photomultipliers/product/p9266b-series](https://et-enterprises.com/products/photomultipliers/product/p9266b-series) (consulté le 19 avril 2021).
- 407 [10] « DT5730 », *CAEN - Tools for Discovery*. <https://www.caen.it/products/dt5730/> (consulté le 5 mai
408 2019).
- 409 [11] R. Aryaeinejad, J. K. Hartwell, et D. F. Spencer, « Comparison Between Digital and Analog Pulse
410 Shape Discrimination Techniques for Neutron and Gamma Ray Separation », in *IEEE Nuclear*
411 *Science Symposium Conference Record, 2005*, Wyndham El Conquistador Resort, Puerto Rico,
412 2005, vol. 1, p. 500-504. doi: 10.1109/NSSMIC.2005.1596302.
- 413 [12] C. S. Sosa, M. Flaska, et S. A. Pozzi, « Comparison of analog and digital pulse-shape-
414 discrimination systems », *Nucl. Instrum. Methods Phys. Res. Sect. Accel. Spectrometers Detect.*
415 *Assoc. Equip.*, vol. 826, p. 72-79, août 2016, doi: 10.1016/j.nima.2016.03.088.
- 416 [13] « ROOT a Data analysis Framework | ROOT a Data analysis Framework », 6 mai 2019.
417 <https://root.cern.ch/> (consulté le 6 mai 2019).
- 418 [14] V. Gressier *et al.*, « AMANDE: a new facility for monoenergetic neutron fields production
419 between 2 keV and 20 MeV », *Radiat. Prot. Dosimetry*, vol. 110, n° 1-4, Art. n° 1-4, août 2004,
420 doi: 10.1093/rpd/nch185.
- 421 [15] I. Murata, I. Tsuda, R. Nakamura, S. Nakayama, M. Matsumoto, et H. Miyamaru, « Neutron and
422 gamma-ray source-term characterization of AmBe sources in Osaka University », *Prog. Nucl. Sci.*
423 *Technol.*, vol. 4, p. 345-348, 2014, doi: 10.15669/pnst.4.345.
- 424 [16] « NUCLÉIDE-LARA on the web (2020) ». <http://www.nucleide.org/Laraweb/index.php>
425

- 426 [17]R. Cherubini, G. Moschini, R. Nino, R. Policroniades, et A. Varela, « Gamma calibration of
427 organic scintillators », *Nucl. Instrum. Methods Phys. Res. Sect. Accel. Spectrometers Detect.*
428 *Assoc. Equip.*, vol. 281, n° 2, p. 349-352, sept. 1989, doi: 10.1016/0168-9002(89)91332-6.
- 429 [18]G. Dietze, « Energy calibration of NE-213 scintillation counters by δ -rays », *IEEE Trans. Nucl.*
430 *Sci.*, vol. 26, n° 1, p. 398-402, févr. 1979, doi: 10.1109/TNS.1979.4329665.
- 431 [19]A. A. Naqvi, F. Z. Khiari, A. Coban, A. Aksoy, et A. M. Al-Jalal, « Pulse height resolution of
432 organic scintillators for monoenergetic gamma rays », in *IEEE Conference on Nuclear Science*
433 *Symposium and Medical Imaging*, oct. 1992, p. 4-6 vol.1. doi: 10.1109/NSSMIC.1992.301166.
- 434 [20]Y. Jie, L. Rong, L. Cheng, J. Li, L. Xin-Xin, et Z. Tong-Hua, « Energy calibration of a BC501A
435 liquid scintillator using a γ - γ coincidence technique », *Chin. Phys. C*, vol. 34, n° 7, p. 993-997,
436 juill. 2010, doi: 10.1088/1674-1137/34/7/012.
- 437 [21]N. V. Kornilov, I. Fabry, S. Oberstedt, et F.-J. Hamsch, « Total characterization of neutron
438 detectors with a 252Cf source and a new light output determination », *Nucl. Instrum. Methods*
439 *Phys. Res. Sect. Accel. Spectrometers Detect. Assoc. Equip.*, vol. 599, n° 2-3, p. 226-233, févr.
440 2009, doi: 10.1016/j.nima.2008.10.032.
- 441 [22]L. Stevanato *et al.*, « Light output of EJ228 scintillation neutron detectors », *Appl. Radiat. Isot.*,
442 vol. 69, n° 2, Art. n° 2, févr. 2011, doi: 10.1016/j.apradiso.2010.10.022.
- 443 [23]A. Enqvist, C. C. Lawrence, B. M. Wieger, S. A. Pozzi, et T. N. Massey, « Neutron light output
444 response and resolution functions in EJ-309 liquid scintillation detectors », *Nucl. Instrum.*
445 *Methods Phys. Res. Sect. Accel. Spectrometers Detect. Assoc. Equip.*, vol. 715, p. 79-86, juill.
446 2013, doi: 10.1016/j.nima.2013.03.032.
- 447 [24]H. Wang, D. Carter, T. N. Massey, et A. Enqvist, « Neutron light output function and resolution
448 investigation of the deuterated organic liquid scintillator EJ-315 », *Radiat. Meas.*, vol. 89, p.
449 99-106, juin 2016, doi: 10.1016/j.radmeas.2016.03.009.
- 450 [25]K. F. Flynn, L. E. Glendenin, E. P. Steinberg, et P. M. Wright, « Pulse height-energy relations for
451 electrons and alpha particles in a liquid scintillator », *Nucl. Instrum. Methods*, vol. 27, n° 1, p.
452 13-17, avr. 1964, doi: 10.1016/0029-554X(64)90129-6.
- 453 [26]R. A. Weldon, J. M. Mueller, P. Barbeau, et J. Mattingly, « Measurement of EJ-228 plastic
454 scintillator proton light output using a coincident neutron scatter technique », *Nucl. Instrum.*
455 *Methods Phys. Res. Sect. Accel. Spectrometers Detect. Assoc. Equip.*, vol. 953, p. 163192, févr.
456 2020, doi: 10.1016/j.nima.2019.163192.
- 457 [27]D. B. Pelowitz *et al.*, « MCNPX 2.7.0 extensions », LA-UR-11-02295, LA-UR-11-2295,
458 1058045, avr. 2011. doi: 10.2172/1058045.
- 459 [28]G. Dietze et H. Klein, « Gamma-calibration of NE 213 scintillation counters », *Nucl. Instrum.*
460 *Methods Phys. Res.*, vol. 193, n° 3, p. 549-556, mars 1982, doi: 10.1016/0029-554X(82)90249-X.
- 461 [29]Z. Janout, S. Pospíšil, et M. Vobecký, « Observation of a Doppler broadening of the 4438 keV
462 gamma-line of ^{12}C in processes $^{12}\text{C}(n, n'\gamma)^{12}\text{C}$ and $^9\text{Be}(\alpha, n\gamma)^{12}\text{C}$ », *J. Radioanal. Chem.*, vol.
463 56, no 1, p. 71-81, mars 1980, doi: 10.1007/BF02516939.
- 464 [30]S. A. Pozzi, E. Padovani, et M. Marseguerra, « MCNP-PoliMi: a Monte-Carlo code for correlation
465 measurements », *Nucl. Instrum. Methods Phys. Res. Sect. Accel. Spectrometers Detect. Assoc.*
466 *Equip.*, vol. 513, n° 3, Art. n° 3, nov. 2003, doi: 10.1016/j.nima.2003.06.012.
- 467 [31]E. C. Miller, S. D. Clarke, M. Flaska, S. Prasad, S. A. Pozzi, et E. Padovani, « MCNPX-PoliMi
468 Post-Processing Algorithm for Detector Response Simulations », p. 10.
- 469 [32]C. B. Sivels, S. D. Clarke, E. Padovani, A. M. Prinke, J. I. McIntyre, et S. A. Pozzi, « Validation
470 of MCNPX-PoliMi code for simulations of radionuclide beta-gamma coincidence detection »,
471 *Nucl. Instrum. Methods Phys. Res. Sect. Accel. Spectrometers Detect. Assoc. Equip.*, vol. 906, p.
472 43-49, oct. 2018, doi: 10.1016/j.nima.2018.07.089.
- 473 [33]M. Matzke, « Unfolding procedures », *Radiat. Prot. Dosimetry*, vol. 107, n° 1-3, p. 155-174, nov.
474 2003, doi: 10.1093/oxfordjournals.rpd.a006384.
- 475 [34]M. Reginatto, « Overview of spectral unfolding techniques and uncertainty estimation », *Radiat.*
476 *Meas.*, vol. 45, n° 10, p. 1323-1329, déc. 2010, doi: 10.1016/j.radmeas.2010.06.016.
- 477 [35]X. Xie, X. Yuan, X. Zhang, T. Fan, J. Chen, et X. Li, « Calibration and Unfolding of the Pulse
478 Height Spectra of Liquid Scintillator-Based Neutron Detectors Using Photon Sources », *Plasma*
479 *Sci. Technol.*, vol. 14, n° 6, p. 553-557, juin 2012, doi: 10.1088/1009-0630/14/6/27.

- 480 [36]H. Klein, « Neutron spectrometry in mixed fields: NE213/BC501A liquid scintillation
481 spectrometers », *Radiat. Prot. Dosimetry*, vol. 107, n° 1-3, p. 95-109, nov. 2003, doi:
482 10.1093/oxfordjournals.rpd.a006391.
- 483 [37]Y. Chen *et al.*, « Unfolding the fast neutron spectra of a BC501A liquid scintillation detector
484 using GRAVEL method », *Sci. China Phys. Mech. Astron.*, vol. 57, n° 10, p. 1885-1890, oct.
485 2014, doi: 10.1007/s11433-014-5553-7.
- 486 [38]W. Dep. 6, « Cyclotron », 27 avril 2016. [https://www.ptb.de/cms/en/ptb/fachabteilungen/abt6/fb-](https://www.ptb.de/cms/en/ptb/fachabteilungen/abt6/fb-64/641-ion-accelerators/cyclotron.html)
487 [64/641-ion-accelerators/cyclotron.html](https://www.ptb.de/cms/en/ptb/fachabteilungen/abt6/fb-64/641-ion-accelerators/cyclotron.html) (consulté le 4 janvier 2021).
- 488 [39]A. Öhrn *et al.*, « Calibration procedure for a neutron monitor at energies below 20MeV », *Nucl.*
489 *Instrum. Methods Phys. Res. Sect. Accel. Spectrometers Detect. Assoc. Equip.*, vol. 592, n° 3, p.
490 405-413, juill. 2008, doi: 10.1016/j.nima.2008.04.030.
- 491 [40]C. C. Lawrence, M. Febraro, T. N. Massey, M. Flaska, F. D. Becchetti, et S. A. Pozzi, « Neutron
492 response characterization for an EJ299-33 plastic scintillation detector », *Nucl. Instrum. Methods*
493 *Phys. Res. Sect. Accel. Spectrometers Detect. Assoc. Equip.*, vol. 759, p. 16-22, sept. 2014, doi:
494 10.1016/j.nima.2014.04.062.
- 495 [41]H. Bai *et al.*, « Simulation of the neutron response matrix of an EJ309 liquid scintillator », *Nucl.*
496 *Instrum. Methods Phys. Res. Sect. Accel. Spectrometers Detect. Assoc. Equip.*, vol. 886, p.
497 109-118, avr. 2018, doi: 10.1016/j.nima.2017.12.072.
- 498 [42]R. A. Weldon *et al.*, « Characterization of stilbene's scintillation anisotropy for recoil protons
499 between 0.56 and 10 MeV », *Nucl. Instrum. Methods Phys. Res. Sect. Accel. Spectrometers*
500 *Detect. Assoc. Equip.*, vol. 977, p. 164178, oct. 2020, doi: 10.1016/j.nima.2020.164178.
- 501 [43]W. Steinberger, N. Giha, M. Hua, S. Clarke, et S. Pozzi, « Anisotropic neutron response of trans-
502 stilbene and impact on a handheld dual particle imager », *Nucl. Instrum. Methods Phys. Res. Sect.*
503 *Accel. Spectrometers Detect. Assoc. Equip.*, vol. 1003, p. 165266, juill. 2021, doi:
504 10.1016/j.nima.2021.165266.
505

Captions with figures sizes

Figure 1 (Full color online): Picture of the coincidence experimental set-up.

(Size H 83.3 mm L 140)

Figure 2 (Full color online): Comparison between the experimental spectra with (w: red solid line) and without (w/o: blue solid line) the coincidence method for: ^{207}Bi (a) and ^{60}Co (b).

(Size H 74.4 mm L 190 mm)

Figure 3: Normalized and smoothed response given by ^{137}Cs (black square) and its first order derivate (white square). The intersection between the experimental spectrum and the dotted line representing the centroid of the Gaussian distribution indicates the assumed CE position.

(Size H 70.1 mm L 85 mm)

Figure 4 (Full color online): Comparison of the energy calibration curves for high (a.1) and low (a.2) gamma energies; the larger error bars's size is comparable with the symbol one. (b.1) Comparison between $^{12}\text{C}^*$ experimental calibrated spectra using L_{Mean} (black solid line) and L_{High} (blue solid line). (b.2) Comparison between ^{241}Am experimental calibrated spectra using L_{Mean} (black solid line) and L_{Low} (red solid line) and the simulated spectrum (blue dashed line) using MCNPX (see Section 4).

(Size H 180.5 mm L 185 mm)

Figure 5 (Full color online): (Left) Comparison of the stilbene calibration data points obtained without (w/o: black solid square) and with (w: black empty square) the coincidence method; the larger error bars's size is comparable with the symbol one. Calibration points have been fitted using Eq. (1) (dashed line) in the energy range between 0.3 and 2 MeV and Eq. (2) (solid line) in the energy range between 0 and 0.3 MeV. For the calibration curves color is used: red for the curve obtained with the coincidence method and blue without it. (Right) Comparison between experimental calibrated spectra for ^{60}Co using L_{Mean} parameters obtained with (blue solid line) and without (red solid line) the coincidence data.

(Size H 80.3 mm L 190 mm)

Figure 6: Energy resolution (a) curve of the stilbene obtained using Eq. (5). FWHM (b) curve of the stilbene obtained using Eq. (3) (black solid line) and $a\sqrt{E}$ (black dashed line) with $a = (8.12 \pm 0.51) \times 10^{-2}$. For both data sets, the larger error bars's size is comparable with the symbol one.

(Size H 79.6 mm L 185 mm)

Figure 7 (Full color online): Comparison between simulated (dashed black line) and experimental calibrated (solid blue line) spectra for ^{22}Na (a) and ^{207}Bi (b).

(Size H 77 mm L 190 mm)

Figure 8 (Full color online): Comparison between the experimental spectrum found with the coincidence method and the corresponding simulated spectra obtained with MCNPX-Polimi for: ^{60}Co (a) and ^{152}Eu (b).

(Size H 77 mm L 190 mm)

Figure 9 (Full color online): Calculated efficiency curves, according to Eq. (7), for $\text{Ø}25.4 \times 25.4 \text{ mm}^3$ stilbene with several thresholds (solid lines). Experimental efficiencies were obtained with a source of ^{137}Cs (black solid squares).

(Size H 77 mm L 85 mm)

Figure 10: Full color online): Comparison between the stilbene unfolded spectra and the expect gamma peaks for: $^{12}\text{C}^*$ (a) and ^{152}Eu (b).

(Size H 77 mm L 190 mm)

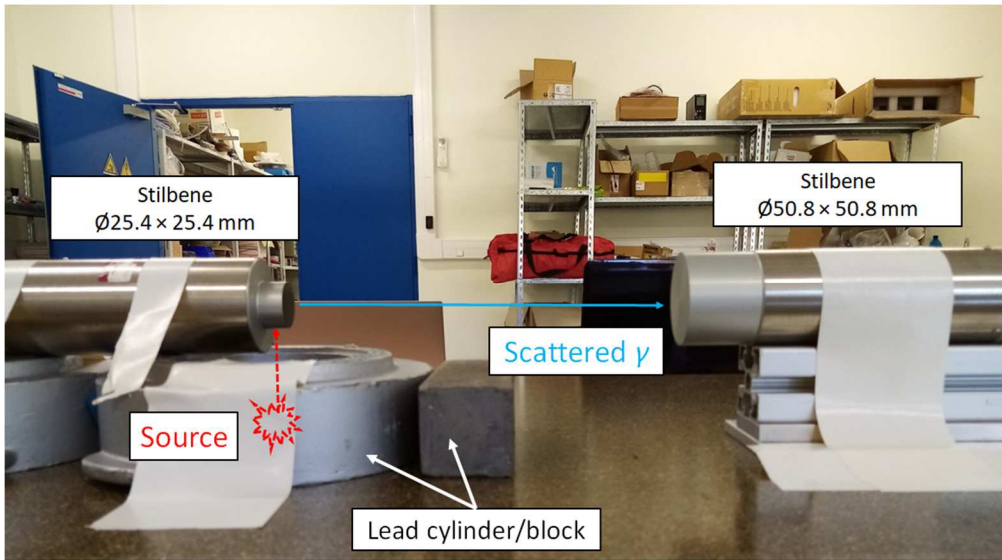


Figure 1

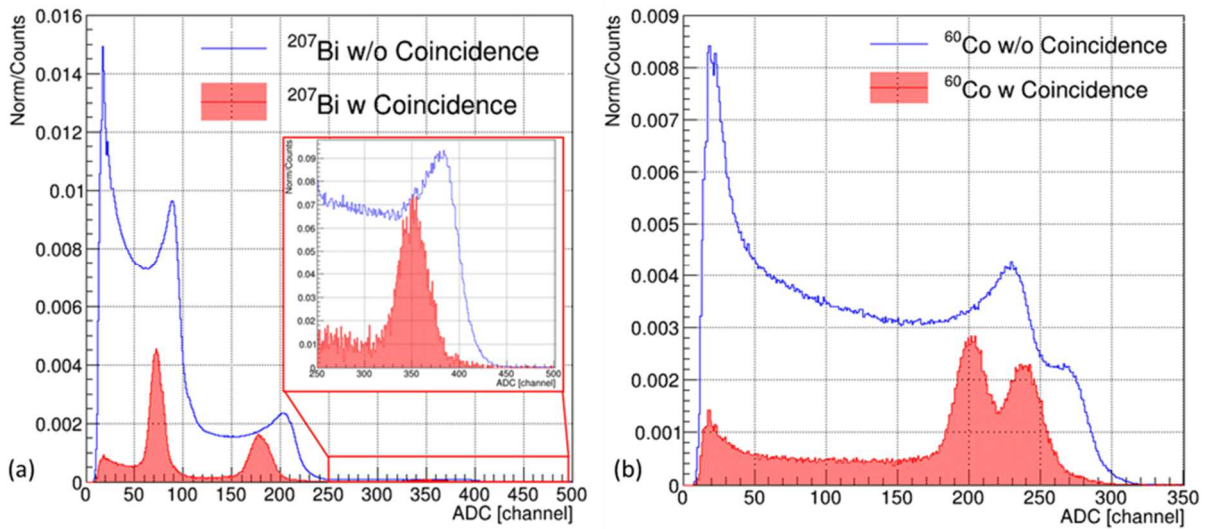


Figure 2

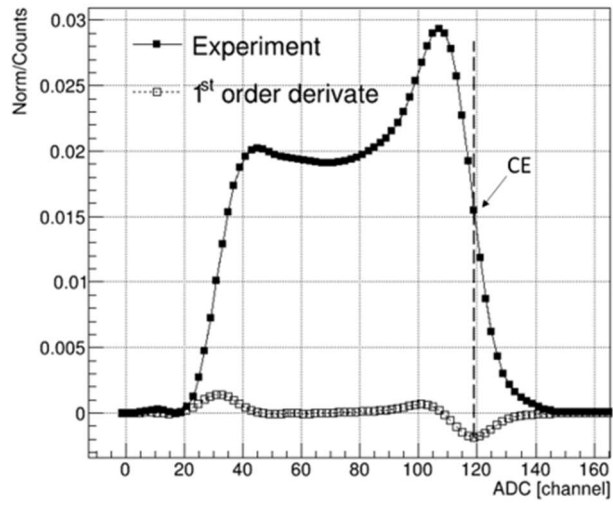


Figure 3

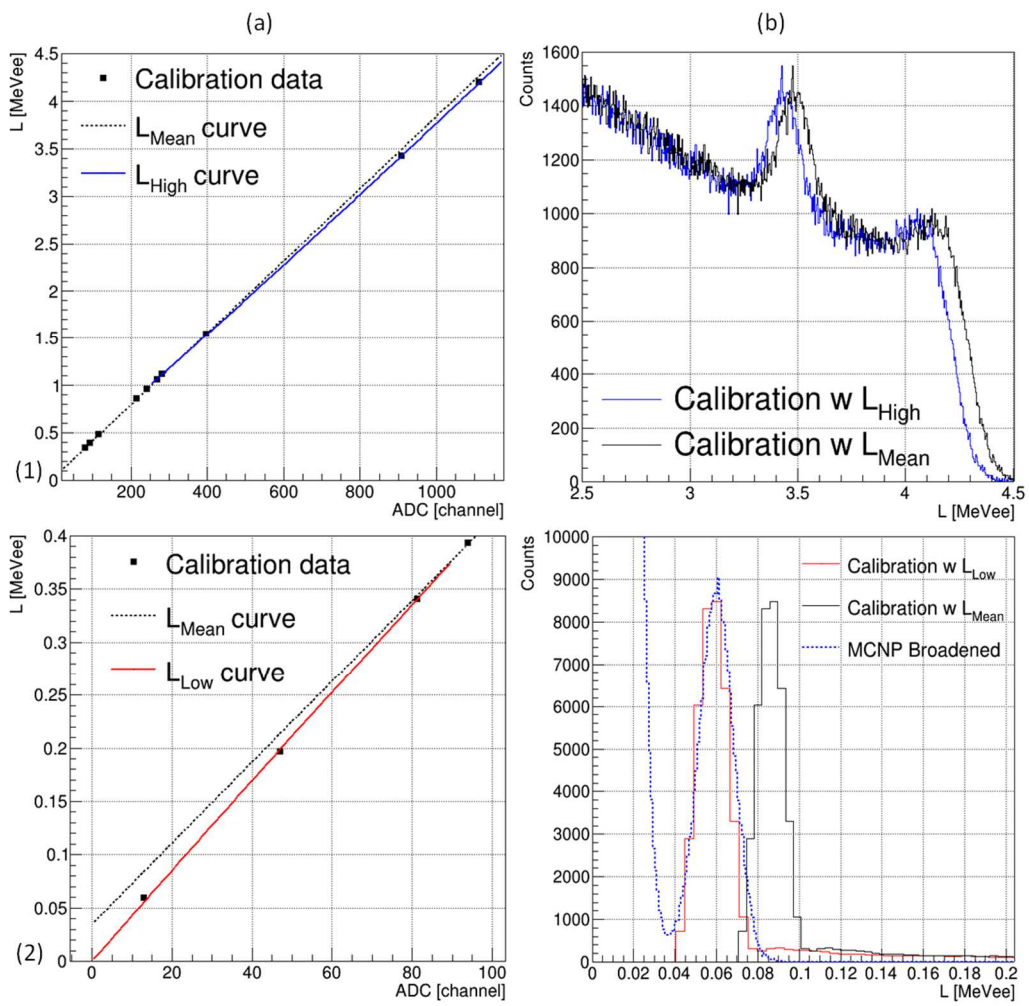


Figure 4

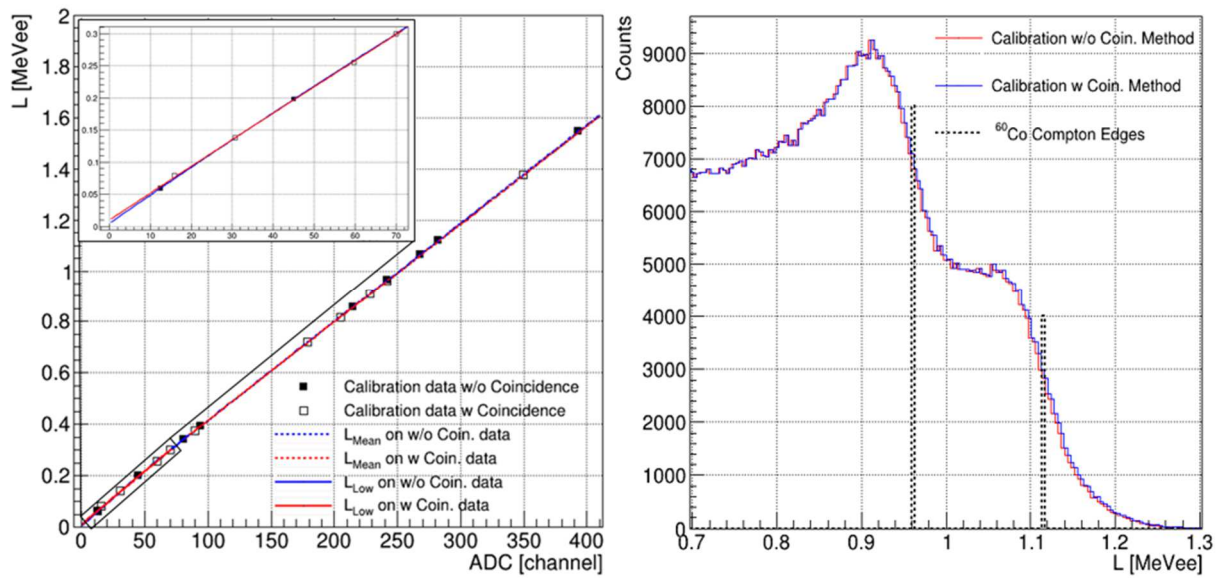


Figure 5

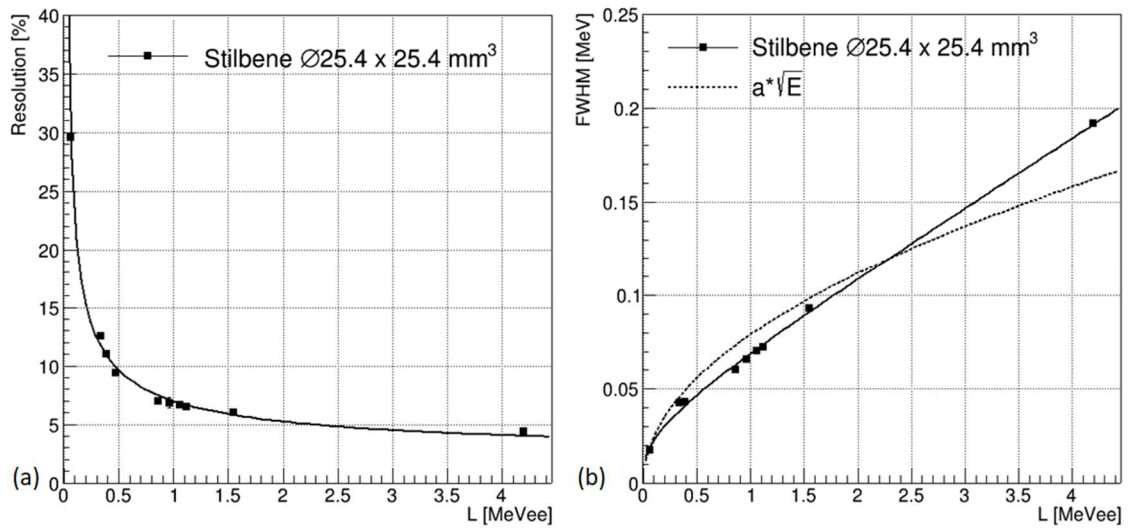


Figure 6

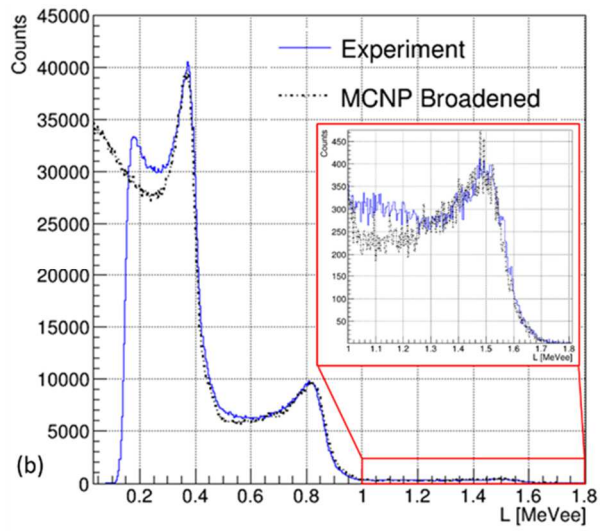
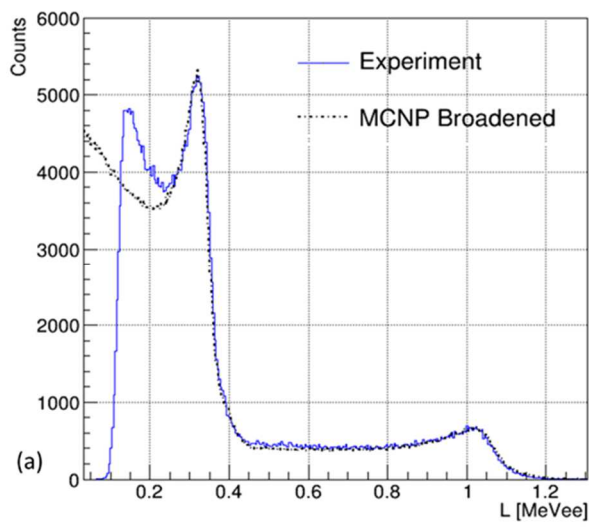


Figure 7

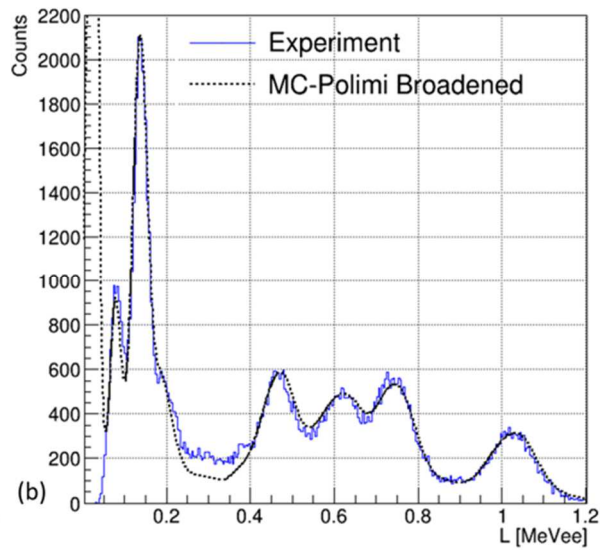
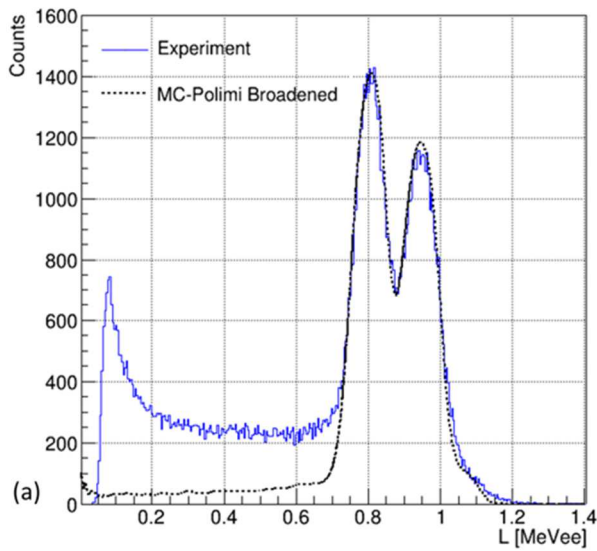


Figure 8

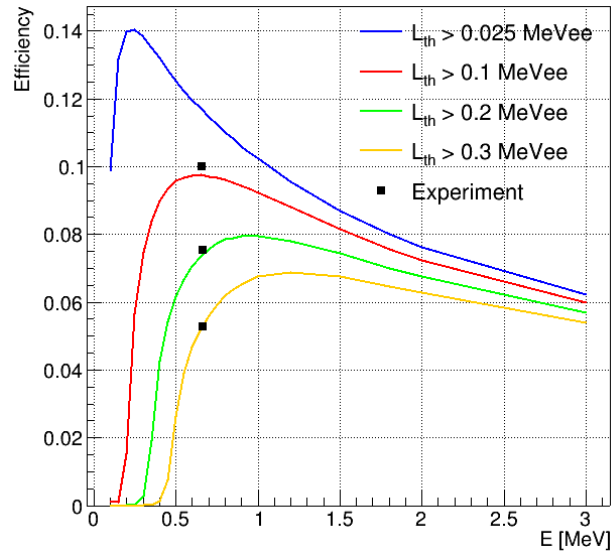


Figure 9

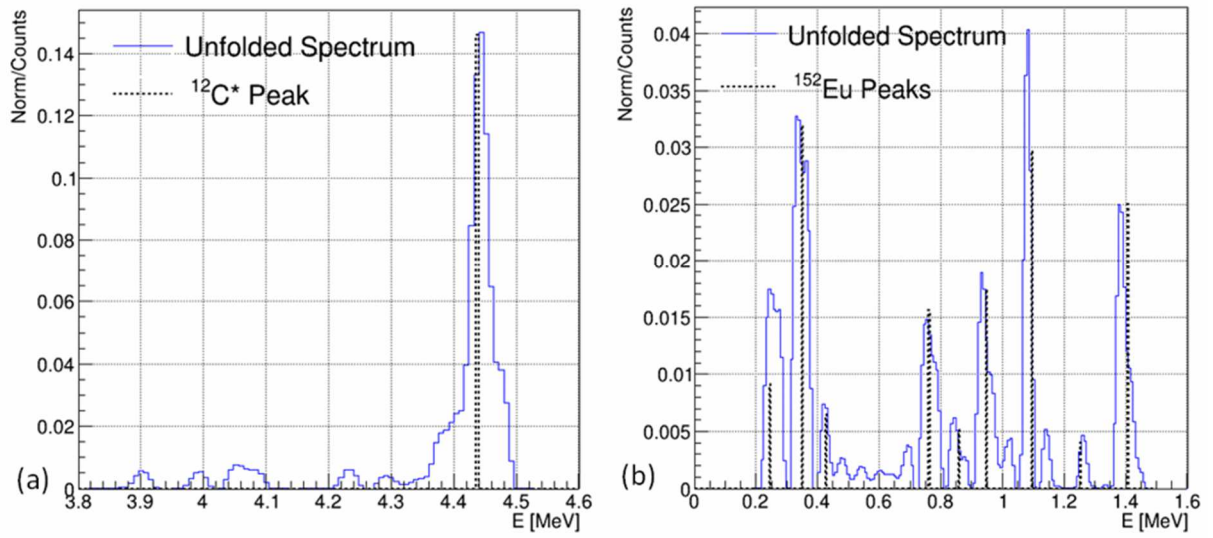


Figure 10

Tables

Table 1: Characteristics of organic scintillators used in this work. The grey line indicates the stilbene detector under study.

Organic scintillator model	Type	Diameter [mm]	Length [mm]	Density [g/cm ³]	Photomultiplier model	Photomultiplier's voltage [V]
Stilbene	Crystal	25.4	25.4	1.15	ET-9214B [8]	-930
Stilbene	Crystal	50.8	50.8	1.15	ET-9266B [9]	-1100

Table 2: Gamma radionuclides used for the stilbene energy calibration, E_γ corresponds to the energy peaks produced by the sources, while E_{re} is the Compton edge energy (180° or 90° recoil electrons). Peak intensities were taken from the LARA library [16]. Sources with a grey background were used in coincidence measurements.

Source	E_γ [keV]	$E_{re}(180^\circ)$ [keV]	$E_{re}(90^\circ)$ [keV]	Intensity [%]	Source activity [kBq]
²⁴¹ Am	59.6	Photoelectric interaction		35.92	-
¹³⁷ Cs	662	478	373	84.99	422.3
²² Na	1275 511	1062 341	910 256	99.94 180.7	421
⁶⁰ Co	1332 1173	1117 963	962 817	99.9826 99.85	387.2
²⁰⁷ Bi	1770 1063 570	1547 857 394	1374 718 301	6.871 74.58 97.76	384
¹⁵² Eu	344 244	197 120	138 79	26.5 7.58	480
¹² C*	4438	4196	3980	85	16.5

Table 3: Stilbene detector calibration parameters with and without the coincidence method for two energy intervals. The L_{Low} parameters are obtained using Eq. (2) while L_{Mean} uses Eq. (1).

	Without the coincidence		With the coincidence	
	L_{Low} [0, 0.3] MeV	L_{Mean} [0.3, 2] MeV	L_{Low} [0, 0.3] MeV	L_{Mean} [0.3, 2] MeV
a	$(0.69 \pm 0.89) \times 10^{-2}$	$(2.93 \pm 0.11) \times 10^{-2}$	$(0.81 \pm 0.27) \times 10^{-2}$	$(2.9 \pm 0.3) \times 10^{-2}$
b	$(44.24 \pm 6.57) \times 10^{-4}$	$(38.56 \pm 0.04) \times 10^{-4}$	$(42.23 \pm 0.65) \times 10^{-4}$	$(38.63 \pm 0.17) \times 10^{-4}$
c	$(-4.95 \pm 8.71) \times 10^{-6}$	-	$(-1.27 \pm 0.24) \times 10^{-6}$	-

Table 4: Experimental parameters of equations (5) and (3).

$R(L(E))$			$FWHM(E)$		
α [%]	β [%]	γ [%]	a' [MeV]	b' [MeV ^{1/2}]	c' [MeV ⁻¹]
2.4 ± 0.7	6.52 ± 0.27	0.7 ± 0.1	0.006 ± 0.003	0.051 ± 0.005	0.51 ± 0.13

Table 5: Deviations between experimental and simulated spectra for values on the midpoint (E_{re}) and FWHM of Gaussian curves.

Source	$E_{re}(90^\circ)$ [MeV]	E_{re} Deviation	FWHM Deviation
¹⁵² Eu	0.079	(0.88 ± 0.03)%	(4.98 ± 0.07)%
¹⁵² Eu	0.138	(0.43 ± 0.01)%	(2.92 ± 0.02)%
¹⁵² Eu	0.470	(0.52 ± 0.05)%	(2.82 ± 0.11)%
¹⁵² Eu	0.630	(-0.47 ± 0.11)%	(7.00 ± 0.36)%
¹⁵² Eu*	0.750	(-0.57 ± 0.08)%	(2.24 ± 0.27)%
⁶⁰ Co	0.817	(-0.27 ± 0.04)%	(1.66 ± 0.14)%
⁶⁰ Co	0.962	(-0.09 ± 0.07)%	(1.59 ± 0.09)%
¹⁵² Eu	1.033	(-0.40 ± 0.05)%	(3.88 ± 0.01)%

(*The 0.75 MeV measurement corresponds to the average of the 1.085, 1.089 and 1.112 MeV gamma rays, which cannot be separated due to the limited resolution of the detector and of the experimental setup .)

Table 6: Deviation in mean energy value and intensity between the unfolded experimental spectra and theoretical values.

	Gamma Energy (MeV)	Intensity (%)	Mean energy deviation	Intensity deviation
¹⁵² Eu	0.244	7.55	-0.20%	87.92%
¹⁵² Eu	0.344	26.59	0.29%	0%
¹⁵² Eu*	0.4275 (0.411/0.444)	5.358 (2.238/3.12)	0.23%	6.36%
¹⁵² Eu	0.778	12.97	0.13%	-6.96%
¹⁵² Eu	0.867	4.24	0.69%	17.03%
¹⁵² Eu	0.964	14.5	0.73%	5.12%
¹⁵² Eu*	1.0953 (1.085/1.089/1.112)	25.27 (10.13/1.73/13.41)	0.43%	31.76%
¹⁵² Eu*	1.2555 (1.212/1.299)	3.04 (1.41/1.63)	-0.83%	7.15%
¹⁵² Eu	1.408	20.85	0.75%	-2.17%
¹² C*	4.438	85	-0.24%	-